Liquid Crystals
Publication details, including instructions for authors and subscription information:
http://www.informaworld.com/smpp/title~content=t713926090

Effect of the semi-fluorinated chiral alkane on the formation of the antiferroelectric phase

Shune-Long Wu[a]; Cho-Ying Lin[a]
[a] Department of Chemical Engineering, Tatung University, Taipei, Taiwan 104, ROC

To cite this Article Wu, Shune-Long and Lin, Cho-Ying(2006) 'Effect of the semi-fluorinated chiral alkane on the formation of the antiferroelectric phase', Liquid Crystals, 33: 4, 495 — 502
To link to this Article: DOI: 10.1080/02678290600633451
URL: http://dx.doi.org/10.1080/02678290600633451

Liquid Crystals, Vol. 33, No. 4, April 2006, 495–502

Effect of the semi-fluorinated chiral alkane on the formation of the antiferroelectric phase

SHUNE-LONG WU* and CHO-YING LIN

Department of Chemical Engineering, Tatung University, 40 Chungshan N. Rd., 3rd Sec.Taipei, Taiwan 104, ROC

(*Received 30 September 2005; accepted 3 January 2006*)

Two structurally similar homologous series of chiral liquid crystals derived from semi-fluorinated and non-fluorinated alkanes positioned at a chiral terminal chain have been synthesized and characterized by differential scanning calorimetry, polarizing optical microscopy and electric-optical measurements. It was found that there are two semi-fluorinated materials in the series I-*m* (*m*=8, 10), that exhibit ferroelectric SmC* and antiferroelectric SmC^*_A phases. The corresponding non-fluorinated materials II-*m* (*m*=8, 10), however, display only the SmC* phase, suggesting that the fluorinated materials encourage the formation of the antiferroelectric SmC^*_A phase. The spontaneous polarization ($\mathbf{P}_s$) and apparent tilt angle (θ) were measured, showing that the semi-fluorinated materials have higher $\mathbf{P}_s$ and θ values than non-fluorinated materials at any reduced temperature below the SmA*–SmC* transition.

1. Introduction

The substitution of fluorine for hydrogen in chiral liquid crystals leads to many interesting phenomena. For example, several studies by different groups show that fluorination of the hydrocarbon chain strongly favours the formation of the smectic phase [1–7]. In addition to its effect on mesophase formation, fluorination has other benefits for liquid crystal materials such as low viscosity, lower birefringence and enhanced chemical stability [8–16]. The fluorine atom has also generally been applied in the design of antiferroelectric liquid crystal materials. The chiral material TFMHPOBC, having the semi-fluorinated alkyl chain trifluoromethyl at the chiral centre of the molecules, has improved thermal stability of the antiferroelectric phase as compared with the structurally similar non-fluorinated material, MHPOBC [17, 18]. Some recent studies indicate that a semi-fluorinated alkane attached to the achiral alkyl chain of liquid crystal molecules leads to the formation of an orthoconic antiferroelectric liquid crystal (OAFLC) that has a 45° tilt angle independent of temperature over a broad temperature range, and which exhibits excellent contrast and grey level scale [19–21].

Our previous study on a series of semi-fluorinated chiral materials MPFPECP*m*BC(*m*=8–12), derived from the semi-fluorinated chiral moiety (*S*)-1-methyl-2-(2,2,3,3,3-pentafluoropropyloxy)ethanol, showed that all the materials possess the antiferroelectric SmC^*_A phase with rather wide temperature ranges [22, 23]. Thus, in order to obtain more detail on the effect of this semi-fluorinated chiral moiety in the formation of the antiferroelectric phase and its corresponding physical properties, in this study, a homologous series of semi-fluorinated chiral materials derived from (*S*)-1-methyl-2-(2,2,3,3,3-pentafluoropropyloxy)ethanol with different core structure from MPFPECP*m*BC was prepared for investigation. A structurally similar homologous series of non-fluorinated chiral materials derived from (*S*)-1-methyl-2-propyloxyethanol was also prepared for comparison. The general structural formulae for both series of materials are depicted below.

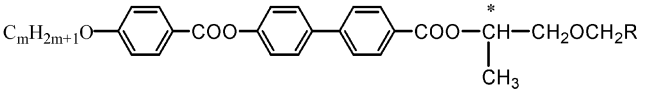

I-m; R= -CF_2CF_3, m=7~12
II-m; R= -CH_2CH_3, m=8~12

2. Experimental

2.1. *Characterization of the materials*

The chemical structures for the intermediates and target materials were determined by nuclear magnetic resonance spectroscopy using a Jeol EX-400 FTNMR spectrometer. The purity was checked by thin layer

*Corresponding author. Email: slwu@ttu.edu.tw

Liquid Crystals
ISSN 0267-8292 print/ISSN 1366-5855 online © 2006 Taylor & Francis
http://www.tandf.co.uk/journals
DOI: 10.1080/02678290600633451

chromatography and further confirmed by elemental analysis using a Perkin-Elmer 2400 spectrometer. Transition temperatures and phase transition enthalpies of the materials were determined by differential scanning calorimetry using a Perkin-Elmer DSC7 calorimeter at running rates of $5^{\circ}C\,min^{-1}$. Mesophases were principally identified by microscopic texture of the materials sandwiched between two glass plates under crossed polarizing microscope using a Nikon Microphot-FXA in conjunction with Mettler FP82 hot stages.

The physical properties of ferroelectric and antiferroelectric phases were measured in 5 μm homogeneously aligned cells, purchased from E. H. C. Co. Japan. The spontaneous polarization ($\mathbf{P}_s$) was measured by a triangular wave method [24]. The measurement of optical transmittance versus applied electric field was conducted using a He-Ne laser (5 mW, 632.8 nm) as a probe beam [25, 26]. The optical transmittance of the probe beam passing though the cell between crossed polarizers, whose axes were parallel and perpendicular to the smectic layer normal, was detected by a photodiode linked to a HP54502A digital oscilloscope. The voltage applied to the electric field was produced by an arbitrary wave-from generator (AG1200) and amplified by a homemade power preamplifier.

2.2. *Preparation of materials*

The starting chiral materials, (*S*)-propylene oxide and 2,2,3,3,3-pentafluoro-1-propanol, were purchased from Aldrich Co. Chem., with purity greater than 99%. Thin layer chromatography was performed with TLC sheets coated with silica; spots were detected by UV irradiation. Silica gel (MN kieselgel 60, 70–230 mesh) was used for column chromatography. Anhydrous organic solvents, dichloromethane (CH_2Cl_2) and tetrahydrofuran (THF), were purified by treatment with CaH_2 and $LiAlH_4$, respectively, and distilled before use.

The synthetic procedures for the target materials I-*m*; (*m*=7–12) and II-*m*; (*m*=8–12) were carried out as outlined in scheme 1. Detailed procedures are described below.

2.2.1. 4-Methoxycarbonyloxyphenylbenzoic acid, 1 [27]. To a solution of sodium hydroxide (7.5 g, 175 mmole) in water (200 ml) which was maintained at

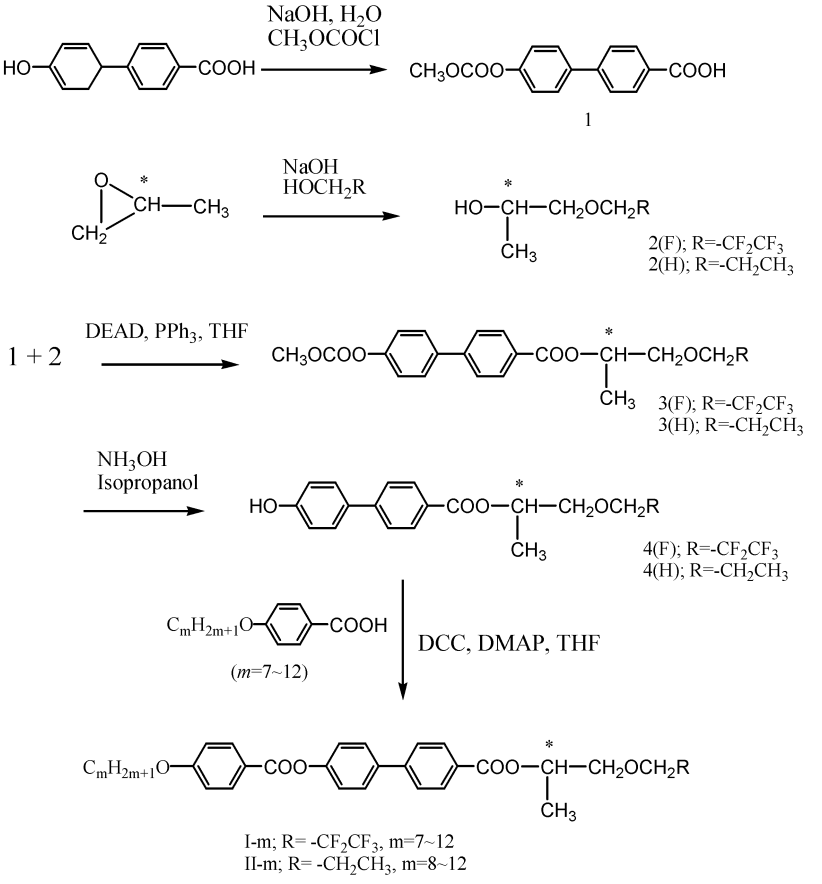

Scheme 1. Procedures for the synthesis of the chiral materials I-*m* (*m*=7–12) and II-*m* (*m*=8–12).

0°C, 4′-hydroxybiphenyl-4-carboxylic acid (13.9 g, 65 mmol) was added with vigorous stirring. Methyl chloroformate (10 g, 105 mmole) was then added slowly to the resulting suspension which was maintained at 0–5°C. The resulting slurry was stirred for a further 4 h and brought to pH 5 by the addition of conc. hydrochloric acid and water (1/1). The voluminous precipitate was filtered off and recrystallized from ethanol to give a white solid; an 80% yield of the material **1** was obtained. ^{1}H NMR (400 MHz, d_6-DMSO): δ(ppm) 3.85–3.87 (s, 3H, OC**H**$_3$), 7.35–7.37 (d, 2H, Ar**H**, J=8.6 Hz), 7.80–7.83 (d, 2H, Ar**H**, J=8.4 Hz), 7.80–7.81 (d, 2H, Ar**H**, J=7.3 Hz), 8.01–8.02 (d, 2H, Ar**H**, J=8.3 Hz), 9.80 (s, 1H, COO**H**).

2.2.2. (*S*)-1-Methyl-2-(2,2,3,3,3-pentafluoropropyloxy) ethanol, 2(F) [28]. 2,2,3,3,3-Pentafluoro-1-propanol (25 g, 16 mmol) and sodium hydroxide (0.1 g, 2.5 mmol) were heated reflux under for 2 h and cooled to room temperature. (*S*)-Propylene oxide (6.38 g, 11 mmol) was added dropwise and the mixture heated under reflux overnight. The resultant mixture was filtered, and excess 2,2,3,3,3-pentafluoro-1-propanol removed under vacuum. The resinous mass thus obtained was distilled under high vacuum to give an 80% yield of pure product, b.p. 80°C/32 torr. ^{1}H NMR ($CDCl_3$, TMS) spectrum for the material 2(F) are: δ(ppm) 1.15–1.17 (d, 3H, –CH*C**H**$_3$, J=8.4 Hz), 2.20–2.21 (s, 1H, –O**H**, J=3.2 Hz), 3.40–3.62 (m, 2H, –CH*C**H**$_2$OCH$_2$–), 3.92–4.01 (m, 3H, –C**H***CH$_3$–, –CH$_2$OC**H**$_2$CF$_2$–)

2.2.3. (S)-1-Propyloxy-2 propanol, 2(H). Material **2(H)** was prepared in an analogous manner to **2(F)**; the yield was 54%. ^{1}H NMR (400 MHz, $CDCl_3$): δ(ppm) 0.90–0.94 (t, 3H, CH$_2$C**H**$_3$, J=7.2 Hz), 1.13–1.51 (d, 3H, CH*C**H**$_3$, J=6.4 Hz), 1.58–1.63 (m, 2H, CH$_2$C**H**$_2$CH$_3$), 2.75 (s, 1H, O**H**, J=3.0), 3.39–3.44 (m, 4H, **CH**$_2$OC**H**$_2$), 3.95–3.96 (m, 1H, HOC**H***CH$_3$).

2.2.4. (*R*)-1-Methyl-2-(2,2,3,3,3-pentafluoropropyloxy) ethyl 4-[4′-(methoxycarbonyloxy)phenyl]benzoate, 3(F) [27]. A solution of diethyl azodicarboxylate (DEAD, 2.2 g, 13 mmol) and material **2(F)** (3.5 g, 13 mmol) in 10 ml anhydrous THF was added dropwise to a solution of triphenylphosphine (Ph_3P, 3.4 g, 13 mmol) and material **3** (1.96 g, 10 mmol) in anhydrous THF (10 ml) at room temperature with vigorous stirring. The reaction soon started. After standing overnight at room temperature, triphenylphosphine oxide was removed by filtration; THF was removed from the filtrate under vacuum. The products were isolated by column chromatography over silica gel (70–230 mesh) using ethyl acetate/hexane (v/v=2/8) as eluent to give a colourless liquid. A 60% yield of product was obtained and identified by the ^{1}H NMR spectrum. ^{1}H NMR ($CDCl_3$, TMS): δ(ppm) 1.44–1.46 (d, 3H, –CH*C**H**$_3$, J=7.1 Hz), 3.76–3.93 (m, 2H, –CH*C**H**$_2$OCH$_2$–), 3.94 (s, 3H, –OCOOC**H**$_3$,), 3.97–4.01 (m, 2H, –CH$_2$OC**H**$_2$CF$_2$–), 5.26–5.29 (m, 1H, –COOC**H**CH$_3$), 7.27–7.29 (d, 2H, Ar**H**, J=8.8 Hz), 7.62–7.64 (d, 2H, Ar**H**, J=8.4 Hz), 7.62–7.64 (d, 2H, Ar**H**, J=8.4 Hz), 8.08–8.10 (d, 2H, Ar**H**, J=8.4 Hz).

2.2.5. (*R*)-1-Propyloxy-2-propyl 4-[4′-(methoxycarbonyloxy)phenyl]benzoate, 3(H). Material **3(H)** was prepared in an analogous manner to **3(F)**, the yield was 55%. ^{1}H NMR (400 MHz, $CDCl_3$): δ(ppm) 0.89–0.92 (t, 3H, CH$_2$C**H**$_3$, J=7.4 Hz), 1.37–1.39 (d, 2H, –CH*C**H**$_3$, J=6.4 Hz), 1.57–1.61 (m, 2H, –CH$_2$C**H**$_2$CH$_3$), 3.41–3.52 (m, 2H, –**C**H$_2$OC**H**$_2$–), 3.55–3.66 (m, 2H, –**C**H$_2$OC**H**$_2$–), 3.93 (s, 3H, –COOC**H**$_3$), 5.32–5.35 (m, 1H, –OC**H***CH$_3$), 7.27–7.28 (d, 2H, Ar**H**, J=8.6 Hz), 7.61–7.63 (d, 2H, Ar**H**, J=8.1 Hz), 7.62–7.63 (d, 2H, Ar**H**, J=8.6 Hz), 8.10–8.12 (d, 2H, Ar**H**, J=8.3 Hz).

2.2.6. (*R*)-1-Methyl-2-(2,2,3,3,3-pentafluoropropyloxy) ethyl 4-(4′-hydroxyphenyl)benzoate, 4(F). Material **3(F)** (2.77 g, 6 mmol) was stirred in a mixture of isopropanol (90 ml) and ammonia hydroxide solution (28%, 30 ml) at room temperature for 50 min (TLC analysis revealed a complete reaction) and then poured into water (40 ml) with stirring. The product was extracted using dichloromethane (3 × 50 ml). The combined organic extracts were washed with brine (3 × 50 ml), dried ($MgSO_4$), filtered and evaporated to give a colourless oil. The oil was purified by flash column chromatography over silica gel (70–230 mesh) using dichloromethane; the resulting oil was then dried in vacuum, giving a 70% yield of material **4(F)**. ^{1}H NMR ($CDCl_3$, TMS): δ(ppm) 1.44–1.45 (d, 3H, –CH*C**H**$_3$, J=7.4 Hz), 3.72–3.91 (m, 2H, –CH*C**H**$_2$OCH$_2$–), 3.98–4.05 (m, 2H, –CH$_2$OC**H**$_2$CF$_2$–), 4.69 (s, –O**H**) 5.26–5.32 (m, 1H, –COOC**H**CH$_3$), 6.84–6.85 (d, 2H, Ar**H**, J=8.6 Hz), 7.60–7.62 (d, 2H, Ar**H**, J=8.4 Hz), 7.60–7.62 (d, 2H, Ar**H**, J=8.4 Hz), 7.96–7.98 (d, 2H, Ar**H**, J=8.4 Hz).

2.2.7. (*R*)-1-Propyloxy-2-propyl 4-(4′-hydroxyphenyl) benzoate, 4(H). Material **4(H)** was prepared in an analogous manner to **4(F)**; the yield was 68%. ^{1}H NMR (400MHz, $CDCl_3$): δ(ppm) 0.91–0.94 (t, 3H, CH$_2$C**H**$_3$, J=7.0 Hz), 1.39–1.41 (d, 2H, –CH*C**H**$_3$, J=6.8 Hz), 1.56–1.60 (m, 2H, –CH$_2$C**H**$_2$CH$_3$), 3.49–3.60 (m, 2H, –**C**H$_2$OC**H**$_2$–), 3.61–3.70 (m, 2H, –**C**H$_2$OC**H**$_2$–), 4.60 (s, –O**H**), 5.29–5.32 (m, 1H,

–OC**H***CH_3), 6.86–6.87 (d, 2H, Ar**H**, J=8.8 Hz), 7.23–7.24 (d, 2H, Ar**H**, J=8.2 Hz), 7.24–7.25 (d, 2H, Ar**H**, J=8.6 Hz), 7.88–7.89 (d, 2H, Ar**H**, J=8.4 Hz).

2.2.8. (*R*)-4-[1-Methyl-2-(2,2,3,3,3-pentafluoropropyloxy)ethyloxycarbonyl]biphenyl 4′-alkyloxybenzoates, I-*m* (*m*=7–12). A mixture of 4-4′-alkyloxylbenzoic acid (2.8 mmol), material **4(F)** (1.2 g, 3.1 mmol), *N*,*N*′-dicyclohexylcarbodiimide (0.3 g, 2.8 mmol), 4-dimethylaminopyridine (0.05 g, 0.28 mmol) and dry THF (20 ml) was stirred at room temperature for three days. The precipitate was filtered off and the filtrate washed with 5% acetate acid solution (3 × 50 ml), 5% saturated aqueous sodium hydrogen carbonate (3 × 50 ml) and water (3 × 50 ml); it was then dried over anhydrous magnesium sulfate ($MgSO_4$) and concentrated in vacuum. The residue was purified by column chromatography over silica gel (70–230 mesh) using dichloromethane as eluent. After recrystallization from absolute ethanol, a 40–55% yield of the target material was obtained. The chemical shifts of analytical data for compound I-10 are given as typical for the material ^{1}H NMR ($CDCl_3$, TMS): δ(ppm) 0.87–0.90 (t, 3H, –CH_2C**H**$_3$, J=7.2 Hz), 1.28–1.41 (m, 17H, –OCH_2CH_2(C**H**$_2$)$_7$–, –OCH*C**H**$_3$–), 1.80–1.82 (m, 2H, –OCH_2C**H**$_2$–), 3.78–3.82 (m, 2H, –CH***CH**$_2$O–), 3.98–4.02 (m, 4H, –$CH_2OCH_2CF_2$–, –C**H**$_2$OAr–), 5.32–5.38 (m, 1H, –COOC**H***CH_3–) 6.97–6.99 (d, 2H, Ar**H**, J=9.2 Hz), 7.30–7.32 (d, 2H, Ar**H**, J=8.8 Hz), 7.65–7.67 (d, 2H, Ar**H**, J=8.8 Hz), 7.66–7.68 (d, 2H, Ar**H**, J=8.4 Hz), 8.09–8.11 (d, 2H, Ar**H**, J=6.8 Hz), 8.15–8.17 (d, 2H, Ar**H**, J=8.8 Hz). Elemental analysis: calc. for $C_{36}H_{41}F_5O_6$, C 65.05, H 6.22; found, C 64.97, H 6.10%. All the target materials were analysed by elemental analysis with satisfactory results.

2.2.9. (*R*)-4-[(1-Methyl-2-propyloxy)ethyloxycarbonyl] biphenyl 4′-alkyloxybenzoates, II-*m*; (*m*=8–12). Materials II-*m* were prepared in an analogous manner to I-*m*. The yields were 68–75%. ^{1}H NMR (400 MHz, $CDCl_3$): δ(ppm) 0.85–0.93 (m, 6H, –CH_2C**H**$_3$), 1.20–1.63 (m, 19H, CH_2OCH_2C**H**$_2$$CH_3$, OCH_2CH_2(C**H**$_2$)$_7$, –OCH*C**H**$_3$–), 1.80–1.85 (m, 2H, –OCH_2C**H**$_2$), 3.43–3.51 (m, 4H, –CH***CH**$_2$OC**H**$_2$–), 3.55–3.67 (m, 4H, –CH*C**H**$_2$$OCH_2$–), 4.04–4.12 (t, 2H, ArOC**H**$_2$, J=7.1 Hz), 5.31–5.37 (m, 1H, OC**H***CH_3), 6.97–6.99 (d, 2H, Ar**H**, J=8.8 Hz), 7.30–7.31 (d, 2H, Ar**H**, J=8.5 Hz), 7.65–7.66 (d, 2H, Ar**H**, J=8.2 Hz), 7.66–7.67 (d, 2H, Ar**H**, J=8.4 Hz), 8.11–8.13 (d, 2H, Ar**H**, J=8.3 Hz), 8.15–8.17 (d, 2H, Ar**H**, J=8.8 Hz). Elemental analysis: calc. for $C_{36}H_{46}O_6$, C 75.23, H 8.07; found, C 75.12, H 8.03%. All the target materials were analysed by elemental analysis with satisfactory results.

3. Results and discussion

3.1. *Mesomorphic properties*

The mesophases and their corresponding phase transition temperatures for series I-*m* and II-*m* were determined by texture observation using polarizing optical microscopy and differential scanning calorimetry (DSC). The SmA* phase was characterized by the formation of focal-conic texture, and the SmC* phase by the formation of broken focal-conic texture. The SmC^*_α phase is barely detectable by microscopy because its texture is similar to that of the SmC* phase, which may be due to the low tilt angle and helical pitch which increase smoothly with decreasing temperature [29–31]; this anomaly is further observed in the dielectric constant measurement. The SmC^*_A phase appeared as a broken focal-conic texture and was investigated further by the observation of switching current behaviour. The Cr 1 phase was determined by the transition of SmC* or SmC^*_A to Cr1 in the DSC thermograms, in which remarkable first order transitions with large enthalpies (35.4–16.4 kJ mol^{-1}) were detected [32].

The mesophases, transition temperatures, and enthalpies of transition for the two series of materials, I-*m*(*m*=7–12) and II-*m*(*m*=8–12) are listed in tables 1 and table 2, respectively. Two charts plotting transition temperature versus the number of carbon atoms in the achiral chain for the semi-fluorinated and non-fluorinated materials are shown in figures 1 and 2, respectively. All the materials exhibited enantiotropic SmA* and SmC* phases. As the achiral chain length increases, the temperature range of the SmA* phase decreases and the melting point falls. The Cr 1 crystalline phase appears in the I-*m* series as the achiral chain length exceeds 10, but it disappears in the II-*m* series. It was interesting to find that the SmC^*_α phase occurs in the materials I-10, I-11, II-8 and II-10 with rather broad temperature ranges (calc. 10–20°C). The SmC^*_A phase was found in the semi-fluorinated chiral materials I-8 and I-10, while it was absent from the corresponding non-fluorinated materials. Thus the presence of the semi-fluorinated alkyl chain in the chiral tail favours for the formation of the antiferroelectric SmC^*_A phase, as we have observed in the previous materials [22, 23].

3.2. *Switching behaviour*

The physical properties of the materials were measured in 5 μm homogeneous cells. Figure 3 shows the electrical switching response of I-10 under a triangular wave voltage with field frequency and an amplitude of 5 $V_{p\text{-}p}$. The switching current exhibit a single current peak while cooling from 130 to 107°C, similar to the

Table 1. Mesophases, transition temperatures and associated enthalpy data for the chiral materials I-*m* (*m*=7–12).

	Temperature/°C[a]																	
Materials	I		SmA*		SmC^*_α		SmC*			SmC^*_A			Cr 1[b]			Cr 2	m.p.[c]
I-7	•	154.2 [12.7][d]	•		—		126.3 [0.6]	•		—			—		62.9 [51.2]	•	106.6 [58.6]
I-8	•	154.6 [10.4]	•		—		132.2 [0.5]	•	123.8 [e]	•			—		76.1 [44.1]	•	117.6 [53.9]
I-9	•	148.6 [10.8]	•		—		132.9 [0.7]	•		—			—		69.9 [45.3]	•	101.6 [50.1]
I-10	•	142.4 [10.9]	•	130.9 [f]	•		120.6 [0.8]	•	107.7 [0.05]	•		71.9 [18.4]	•		35.7 [35.4]	•	92.1 [48.3]
I-11	•	139.4 [8.7]	•	129.1 [f]	•		111.3 [1.2]	•		—		71.1 [16.8]	•		31.2 [16.4]	•	96.5 [59.8]
I-12	•	134.8 [9.3]	•		—		125.0 [1.0]	•		—		66.5 [6.5]	•		60.9 [24.3]	•	84.6 [70.2]

[a]Rorded by DSC thermograms at cooling rates of 5°C min^{-1}.
[b]Cr refers to crystal.
[c]m.p. refers to melting point taken from DSC thermograms recorded at heating rates of 5°C min^{-1}.
[d]Figures in square brackets denote enthalpies quoted in kJ mol^{-1}.
[e]The enthalpy was too small to be determined by DSC.
[f]The temperature was confirmed by dielectric studies.

Table 2. Mesophases, transition temperatures and associated enthalpy data for the chiral materials II-*m* (*m*=8–12). For key see table 1.

	Temperature/°C[a]									
Materials	I		SmA*		SmC^*_α		SmC*			Cr[b]	m.p.[c]
II-8	•	136.8 [10.7][d]	•	103.7 [f]	•	92.5 [e]	•	41.3 [60.1]	•	94.8 [51.3]
II-9	•	134.8 [11.4]	•		—	102.6 [e]	•	61.7 [53.0]	•	97.7 [53.0]
II-10	•	130.1 [9.6]	•	104.0 [f]	•	82.1 [0.2]	•	47.6 [52.9]	•	72.2 [62.8]
II-11	•	131.8 [11.3]	•		—	107.7 [0.4]	•	45.3 [63.6]	•	73.9 [79.6]
II-12	•	130.8 [9.5]	•		—	108.2 [0.2]	•	65.4 [88.1]	•	83.3 [94.9]

behaviour reported for SmC^*_α and SmC* phase [33]. In the SmC^*_A phase, however, two switching current peaks appeared, similar to a normal SmC^*_A phase [33], supporting the presence of an antiferroelectric SmC^*_A phase.

3.3. *Dielectric constant*

Figure 4 shows the temperature dependence of the dielectric constant ε' for the material I-10 measured at 100 Hz in a 25 µm homogeneous cell. The ε' in the SmA* phase is small. With decreasing temperature, the ε' slightly increases at the SmA* to SmC^*_α transition. In the SmA* phase close to the $SmA^* - SmC^*_\alpha$ transition at about 130.9°C, the dielectric constant is enhanced slightly by the contribution of the tilt angle vibration (soft mode), whereas in the SmC^*_α, ε' is enhanced by the contribution of vibration of the azimuthal molecular motions [33–37] as well as the soft mode. Cooling to the SmC* phase at approximately 100.7°C, the dielectric constant increases rapidly due to the contribution of the Goldstone mode [37]. Thus, the characteristic of the ferroelectric SmC* phase could be well confirmed. The dielectric constant fell to a very low value further cooling from the SmC* phase to the occurrence of the SmC^*_A phase.

3.4. *Electro-optical response*

Electro-optical response was observed under crossed polarizers where the axes of polarizer and analyser were parallel and perpendicular, respectively, to the smectic

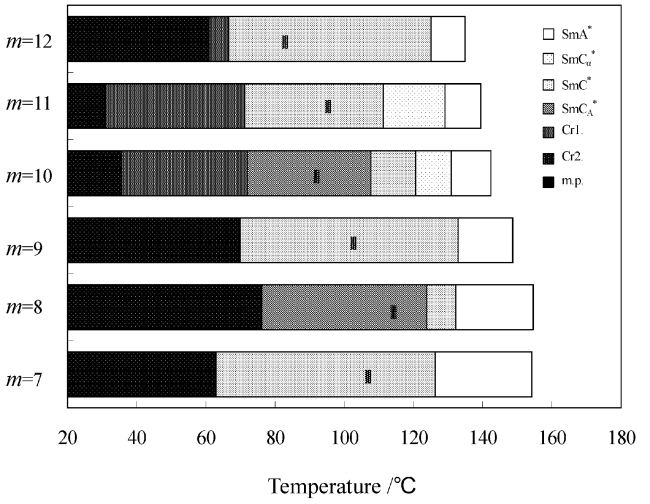

Figure 1. Chart of transition temperature as a function of terminal alkyl chain length for the chiral materials I-*m* (*m*=7–12) on cooling.

layer normal in 5 µm homogeneous by aligned cells. Figure 5 illustrates the variation of transmittance with electric field on application of a triangular waveform field measured in the SmC* and SmC$_A^*$ phase for I-10. It can be seen that at 115°C and 0.5 Hz frequency, an ideal single hysteresis is seen in the SmC* phase, see figure 5 (*a*). However, on cooling to 100°C, an ideal double hysteresis appears in the SmC$_A^*$ phase. This corresponds to a tri-stable switching in the antiferroelectric state, see figure 5 (*b*) [33], and is characteristic of a stable antiferroelectric phase.

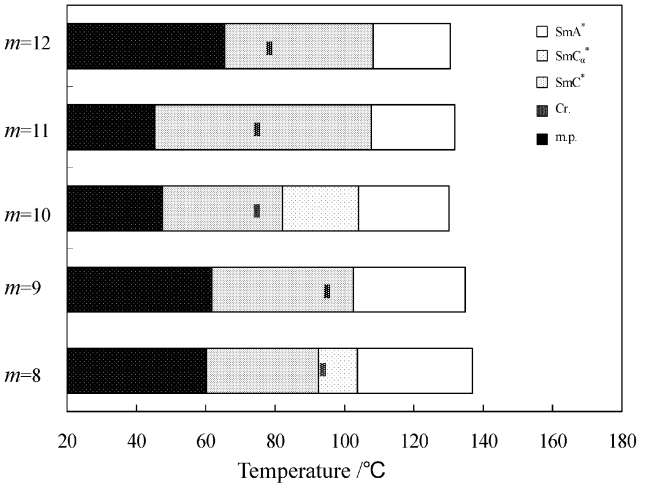

Figure 2. Chart of transition temperature as a function of terminal alkyl chain length for the chiral materials II-*m* (*m*=8–12) on cooling.

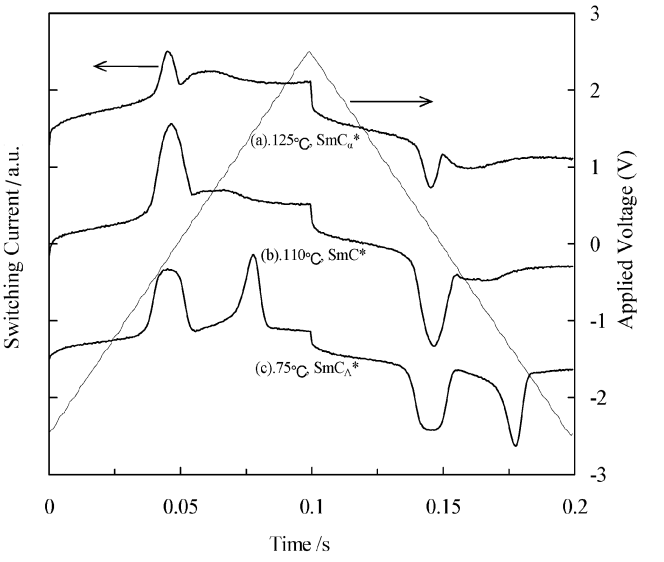

Figure 3. The switching current behaviour of material I-10 obtained at 20 Hz and varied temperature on applying a triangular wave voltage in a 5 µm thick homogeneously aligned cell.

3.5. *Spontaneous polarization and title angle*

The temperature dependence of spontaneous polarization ($\mathbf{P}_s$) for semi-fluorinated materials, I-*m* *m*=9–11 and non-fluorinated materials II-*m* *m*=9–11, is illustrated in figure 6. For the series I-*m*, maximum $\mathbf{P}_s$ values of these materials, which exhibit antiferroelectricity, is in range 95–105 nC cm^{-2}. In contrast, in series II-*m*, the $\mathbf{P}_s$ values are in the smaller range 21–25 nC cm^{-2}, and the materials do not exhibit the SmC$_A^*$ phase. These experimental results imply that the $\mathbf{P}_s$ value is closely related to the polarization of the chiral tail part, which is an important factor in the

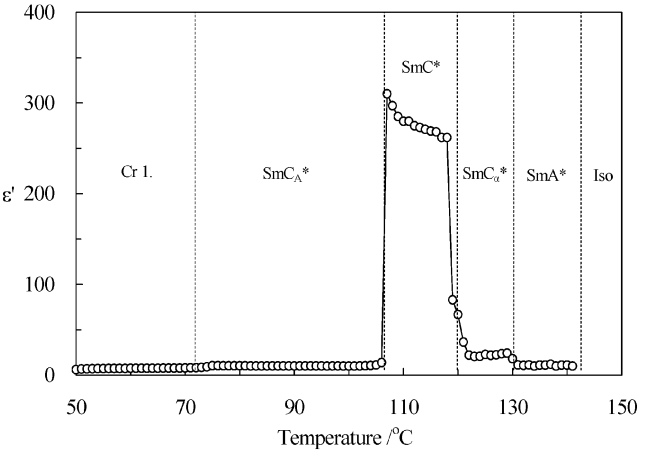

Figure 4. Temperature dependence of dielectric constant (ε′) for the material I-10. Cooling rate 1°C min^{-1}, frequency 100 Hz.

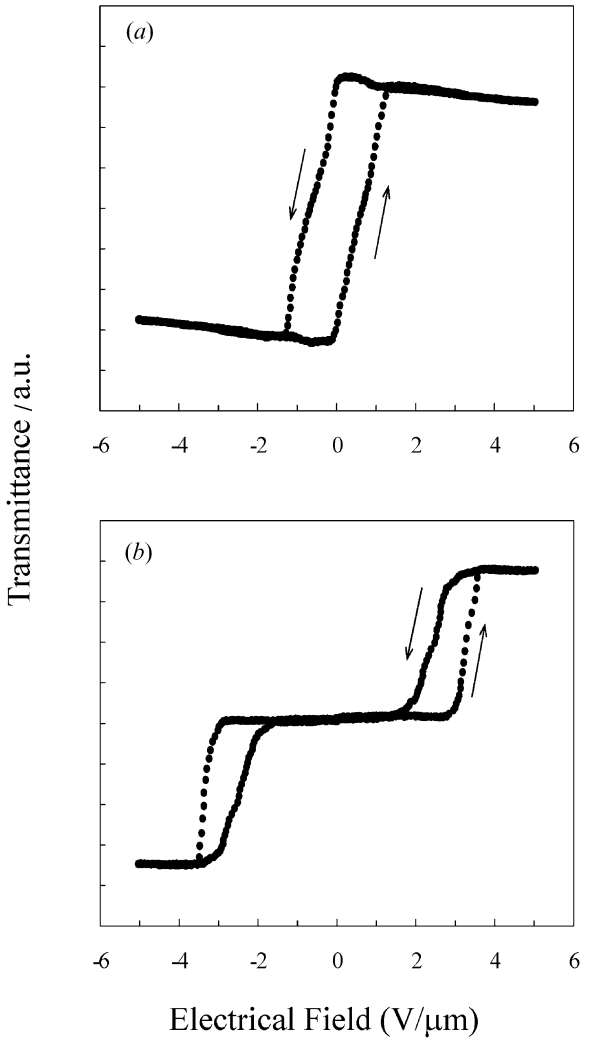

Figure 5. The electro-optical response of material I-10 (*a*) in the SmC* phase at 115°C, (*b*) in the SmC^*_A phase at 100°C and 0.5 Hz frequency of the applyed triangular wave voltage.

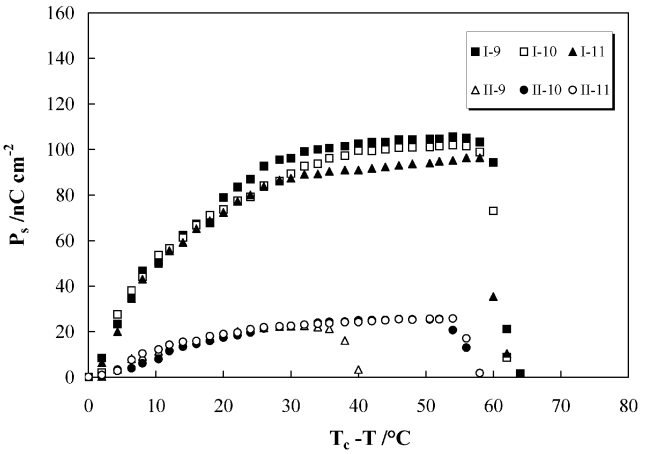

Figure 6. Spontaneous polarization plotted as a function of temperature for the materials I-*m* (*m*=9–11), and II-*m* (*m*=9–11). The T_c is the temperature of the SmA*–SmC* transition.

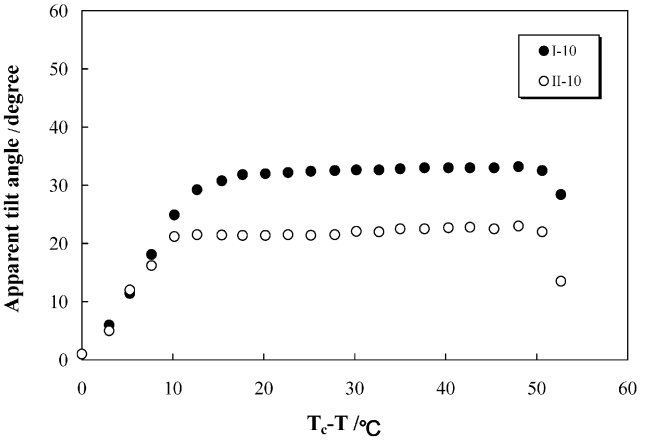

Figure 7. Temperature dependence of apparent tilt angle for the materials I-10 and II-10.

appearance of the antiferroelectricity. Figure 7 shows the temperature dependence of apparent title angle (θ) for materials I-10 and II-10. The maximum title angles values of material I-10 is 33°, while that of material II-10 is 23°C. This indicates that the semi-fluorinated alkane positioned at the chiral tail may increase the tilt angle.

4. Conclusion

We have demonstrated that semi-fluorinated chiral materials I-*m*, derived from (*S*)-1-methyl-2-(2,2,3,3,3-pentafluoropropyloxy)ethanol, display the antiferroelectic SmC^*_A phase in their octyl and decyl members. The semi-fluorinated materials thus favour the formation of the antiferroelectric SmC^*_A phase in comparison with non-fluorinated analogues. Moreover, the transition temperatures, spontaneous polarization and apparent titled angle of the semi-fluorinated materials are significantly larger than those of the non-fluorinated materials. It is worth noting that our previous studies on the semi-fluorinated materials MPFPECP*m*BC showed them all to possess the antiferroelectric SmC^*_A phase [22, 23]. Thus, on comparing the results on the chiral materials I-*m* with those of MPFPECP*m*BC, it can be seen that materials with PhPhCOOPh as the molecular core structure are more likely to form the antiferroelectric SmC^*_A phase than those with PhCOOPhPh as the core structure.

Acknowledgment

The authors are grateful for the financial support of the National Science Council of the Republic of China (NSC 94-2216-E-036-008).

References

[1] S. Takenaka. *Chem. Commun.*, 1748 (1992).
[2] H. Okamoto, H. Murai, S. Takenaka. *Bull. chem. Soc. Jpn.*, **70**, 3163 (1997).
[3] H. Okamoto, N. Yamada, S. Takenaka. *J. Fluorine Chem.*, **91**, 125 (1998).
[4] M. Duan, H. Okamoto, V.F. Petrov, S. Takenaka. *Bull. chem. Soc. Jpn.*, **71**, 2735 (1998).
[5] M. Duan, H. Okamoto, V.F. Petrov, S. Takenaka. *Bull. chem. Soc. Jpn.*, **72**, 1637 (1999).
[6] G. Johansson, V. Percec, G. Ungar, K. Smith. *Chem. Mater.*, **9**, 164 (1997).
[7] G. Fornasieri, F. Guittard, S. Géribaldi. *Liq. Cryst.*, **30**, 663 (2003).
[8] H.T. Nguyen, G. Sigaud, M.F. Achard, F. Hardouin, R.J. Twieg, K. Betterton. *Liq. Cryst.*, **10**, 389 (1991).
[9] P. Kromm, M. Cotrait, H.T. Nguyen. *Liq. Cryst.*, **21**, 95 (1996).
[10] P. Kromm, M. Cotrait, J.C. Rouillon, P. Barois, H.T. Nguyen. *Liq. Cryst.*, **21**, 121 (1996).
[11] H. Liu, H. Nohira. *Liq. Cryst.*, **20**, 581 (1996).
[12] H. Liu, H. Nohira. *Liq. Cryst.*, **22**, 217 (1997).
[13] H. Liu, H. Nohira. *Liq. Cryst.*, **24**, 719 (1998).
[14] E.T. de Givenchy, F. Guittard, F. Bracon, A. Cambon. *Liq. Cryst.*, **26**, 1163 (1999).
[15] E.T. de Givenchy, F. Guittard, F. Bracon, A. Cambon. *Liq. Cryst.*, **26**, 1371 (1999).
[16] H.T. Nguyen, J.C. Rouillon, A. Babeau, J.P. Marcerou, G. Sigaud, M. Cotrait, H. Allouchi. *Liq. Cryst.*, **26**, 1007 (1999).
[17] Y. Suzuki, T. Hagiwara, I. Kawamura. *Liq. Cryst.*, **6**, 167 (1989).
[18] Y. Suzuki, O. Nonaka, Y. Koide, N. Okabe, T. Hagiwara, I. Kawamura, N. Yamamoto, Y. Yamada, T. Kitazume. *Ferroelectrics*, **147**, 109 (1993).
[19] S.T. Lagerwall, A. Dahlgren, P. Jägemalm, P. Rudquist, K. D'havé, H. Pauwels, R. Dąbrowski, W. Drzewinski. *Adv. funct. Mater.*, **11**, 87 (2001).
[20] R. Dąbrowski, J. Gąsowska, J. Otón, W. Pieck, J. Przedmojski, M. Tykarska. *Displays*, **25**, 9 (2004).
[21] P. Perkowski, Z. Raszewski, J. Kędzierski, K. Pieck, J. Rutkowska, S. Kęosowicz, J. Zieliński. *Mol. Cryst. liq. Cryst.*, **411**, 145 (2004).
[22] S.-L. Wu, C.-Y. Lin. *Liq. Cryst.*, **32**, 663 (2005).
[23] S.-L. Wu, C.-Y. Lin, *Liq. Cryst.* (in the press).
[24] K. Miyasato, S. Abe, H. Takezoe, A. Fukuda, E. Kuze. *Jpn. J. appl. Phys.*, **22**, L661 (1983).
[25] A.D.L. Chandani, T. Hagiwara, Y. Suzuki, Y. Ouchi, H. Takazoe, A. Fukuda. *Jpn. J. appl. Phys.*, **27**, L729 (1988).
[26] J. Lee, A.D. Chandani, K. Itoh, Y. Ouchi, H. Takezoe, A. Fukuda. *Jpn. J. appl. Phys.*, **29**, 1122 (1990).
[27] G.J. Booth, A. Dunnur, J.W. Gooby, K.J. Toyne. *Liq. Cryst.*, **28**, 815 (1996).
[28] H.C. Chitwood, B.T. Freure. *J. Am. chem. Soc.*, **68**, 680 (1946).
[29] T. Isozaki, K. Hiraoka, Y. Takanishi, H. Takezoe, A. Fukuda, Y. Suzuki, I. Kawamura. *Liq. Cryst.*, **12**, 59 (1992).
[30] M. Skarabot, M. Cepic, B. Zebs, R. Bling, G. Heppke, A.V. Kityk, I. Masevic. *Phys. Rev. E*, **58**, 575 (1998).
[31] S. Essid, M. Manai, A. Gharbi, J.P. Marcerou, J.C. Rouillon, H.T. Nguyen. *Liq. Cryst.*, **31**, 1185 (2004).
[32] A. Bubnov, V. Hamplová, M. Kašpar, P. Vaněk, D. Pociecha, M. Glogarová. *Mol. Cryst. liq. Cryst.*, **366**, 547 (2001).
[33] A. Fukuda, Y. Takanishi, T. Isozaki, K. Ishikawa, H. Takezoe. *J. mater. Chem.*, **4**, 997 (1994).
[34] K. Hiraoka, A. Taguchi, Y. Ouchi, H. Takezoe, A. Fukuda. *Jpn. J. appl. Phys.*, **29**, L103 (1990).
[35] K. Hiraoka, A.D.L. Chandani, E. Gorecka, Y. Ouchi, H. Takezoe, A. Fukuda. *Jpn. J. appl. Phys.*, **29**, L1473 (1990).
[36] Y. Takanishi, K. Hiraoka, V.K. Agrawal, H. Takezoe, A. Fukuda, M. Matsushita. *Jpn. J. appl. Phys.*, **30**, 2023 (1991).
[37] F. Gouda, K. Skarp, S.T. Lagerwall. *Ferroelectrics*, **113**, 165 (1991).